Received December 19, 2019, accepted January 13, 2020, date of publication January 23, 2020, date of current version January 31, 2020.

*Digital Object Identifier 10.1109/ACCESS.2020.2968931*

# A Bidirectional Absorptive Common-Mode Filter Based on Interdigitated Microstrip Coupled Lines for 5G "Green" Communications

**YANGYANG GUAN[1], YONGLE WU[1], (Senior Member, IEEE), AND MANOS M. TENTZERIS[2], (Fellow, IEEE)**

[1]Beijing Key Laboratory of Work Safety Intelligent Monitoring, School of Electronic Engineering, Beijing University of Posts and Telecommunications, Beijing 100876, China
[2]School of Electrical and Computer Engineering, Georgia Institute of Technology, Atlanta, GA 30332, USA

Corresponding author: Yongle Wu (wuyongle138@gmail.com)

This work was supported in part by the National Natural Science Foundations of China under Grant 61821001 and Grant 61971052, in part by the Beijing Natural Science Foundation under Grant JQ19018, and in part by the BUPT Excellent Ph.D. Students Foundation under Grant CX2019303.

**ABSTRACT** This paper proposes a bidirectional absorptive common-mode filter (A-CMF) for 5G "green" communication systems. The A-CMF is a balanced-to-balanced structure using interdigitated coupled lines to replace normal double parallel-coupled lines for enhanced coupling and easy manufacturing. The resistors are introduced to dissipate the common-mode (CM) noises into heat and thus to avoid the noises being reflected and still existing in the communication system. This novel A-CMF features an intrinsic CM noises absorption while maintaining its differential-mode (DM) filtering characteristics. As a proof-of-concept demonstration, one microstrip prototype is fabricated in a two-layer printed circuit board (PCB) and the measurements are consistent with the simulations. The DM signals can pass through this A-CMF without being attenuated from 1.38 GHz to 5.19 GHz but the CM noises are suppressed throughout the broad frequency range between 0.72 GHz and 8 GHz. It is worth noting that this A-CMF realizes a wide band with 90% absorption efficiency of CM noises from 2.18 GHz to 4.97 GHz.

**INDEX TERMS** Absorptive common-mode filter (A-CMF), common-mode (CM), differential-mode (DM), noise absorption, reflectionless filter, green communication.

## I. INTRODUCTION

Compared to the current 4G network, 5G communication systems need to support higher data rates, much broader bandwidths, and massive connectivity. Thus, it's extremely important to cope with the demands of intense user and energy consumption. Ascending "green" communication approaches not only meets the 5G standards but also benefits the environment and human health. To cater for "green" 5G implementations, numerous technologies for power allocation and energy efficient have been proposed including massive multiple input multiple output (MIMO), internet of things (IoT), ambient energy harvester (EH), and so on.

There will be a strong requirement for massive connectivity in the future IoT and massive MIMO scenarios, where the device activity patterns are typically sporadic. By utilizing compressed sensing techniques, the activities of devices can be easily detected by the base station [1]. In this way, the devices are designed being "hibernating" most of time for saving energy and operate once being activated. In most of the proposed approaches for energy efficient implementations, the main attention has been paid on optimizing the allocation. In addition, sensors forming the wireless sensing networks in the IoT are typically in very large numbers while being power hungry. Energy self-sustaining wireless sensing networks have been presented and an EH has been designed to simultaneously illuminate RFID tags with the output RF second harmonic signal and drive a RF amplifier with the output dc power [2]. Noting that it's the first time the proposed RF EH utilizes not only the dc power but also the second harmonic signal. A wearable EH has also been reported, which can harvest high RF energy and transfer

The associate editor coordinating the review of this manuscript and approving it for publication was Xiu Yin Zhang.

the "hotspots" energy into high dc voltage and power [3]. Plus, a wideband and high gain antenna has been proposed for low energy density far-field RF energy harvesting [4]. Through those energy-saving techniques, the EH "recycles" ambient RF energy and realizes energy autonomy. Therefore, noise suppression and noise absorption techniques over wide frequency ranges have attracted an increasing attention since the common-mode (CM) noises are a kind of RF energy commonly existing in communication systems.

High-frequency CM noises induce electromagnetic interference (EMI) or radio frequency interference (RFI) emission, which do great harm to the electronic systems especially when they are radiated by antennas. Thus, the noise-induced issues are a great challenge for the massive implementation of truly "green" 5G systems. That is why typical low noise amplifiers are widely researched [5], [6]. Due to the noise figure being a key performance factor for low noise amplifiers, a generalized multiband matching network has been proposed and a triband low noise amplifier has been fabricated using a novel impedance matching structure [5]. By employing a common-gate-common-source balun topology, a broadband low noise amplifier has been also put forward [6]. Furthermore, differential topologies have attracted a significant attention due to their inherent immunity to the environmental noises and electromagnetic interferences.

Many balanced RF front-end components have been introduced including balanced antennas [7], [8], balanced filters [9]–[14], and balanced power dividers [15]–[17]. By using textile substrates, a patch antenna and a low noise amplifier have been integrated into an active receiving antenna with optimized noise characteristics [7]. A self-filtering low-noise horn antenna has been introduced, which can self-filter the captured noises [8]. Based on stepped-impedance resonators (SIRs), balanced bandpass filters feature high selectivity and CM suppression by loading a capacitor or a resistor on the SIR [9]. A balanced bandpass filter has been presented with high CM suppression, tunable operating frequency, and constant bandwidth [10]. A compact differential ultra-wideband bandpass filter has been brought out with CM suppression [11]. Using dual-mode ring resonators, two balanced filters have been proposed with wideband CM suppression capabilities [12]. By introducing an embedded defected ground structure, a varactor- and stub-loaded dumbbell-shaped resonator has been used in a dual-band differential filter for CM suppression [13]. High CM suppression for a balanced dual-band bandpass filter has been acquired by using a planar via-free composite right-/left-handed resonator [14]. A planar compact single-ended-to-balanced power divider has been put up with high suppression of the CM noises [15]. Based on balanced architectures, filtering power dividers have been proposed with broadband CM suppression [16] and enhanced in-band CM suppression [17]. All mentioned balanced components above focus on the CM noise suppression. However, the suppressed CM noises are reflected and still exist in the communication system. The concept of the noise absorption is "green" and

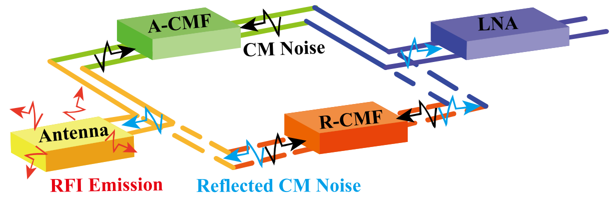


**FIGURE 1.** The schematic diagram of the propagation of CM noises in a RF front-end with R-CMF or A-CMF.

totally different from the noise suppression to an effectively complete extinction of the RF CM noise from the system. Namely, the RF CM noises are used up and no longer existing in the system. The noise absorption technique enables a new form of "green" technologies that the RF components absorb the noise and interference energy.

To address electromagnetic interference and RF interference problems in RF differential systems, several absorptive common-mode circuits have been recommended [18]–[26]. A broadband CM noise absorption circuit has been put forward using resistors for high-speed differential digital systems [18]. Afterwards, several balanced-to-balanced power dividers have been introduced with CM noise absorption characteristic based on resistors [19], [20] and mode-conversion approach [21].

As shown in Fig. 1, the reflective common-mode filter (R-CMF) is normally devised to reflect CM noises back to the previous blocks of circuits. Thus, CM noises inevitably incur RFI problems to further degrade the system performance. In order to implement energy-efficient communication systems, the absorptive common-mode filter (A-CMF) has been invented in recent years to eliminate the reflected CM noises. A planar wideband bandpass filter realizes the function of CM absorption together with the performance of bandpass filtering for the first time [22]. This A-CMF has a consistent bandwidth for both differential-mode (DM) filtering and CM absorption. Hereafter, the CM absorption efficiency at the operating frequency has been defined for the first time and 96% absorption efficiency has been reached using resistors [23]. Instead of using resistors or resistive materials, a resistor-free A-CMF was brought up later using the dielectric loss of PCB for CM noise absorption [24]. Here, a gap-coupled resonator was adopted to achieve noise absorption and was fabricated in a four-layer PCB. All mentioned techniques above realize CM noise absorption by using resistors or lossy dielectric. Nevertheless, the broadband absorption and high absorption efficiency are still very hard to obtain simultaneously. Recently, an A-CMF with a broad 95% absorption band was realized in a four-layer PCB [25]. This approach extended two absorption frequency bands into a single broad band and finally provided 95% absorption efficiency through a wide band. Subsequently, a bidirectional A-CMF was achieved by using a patterned ground structure in a two-layer PCB [26]. Moreover, 98% absorption efficiency and a broadband CM suppression were achieved.

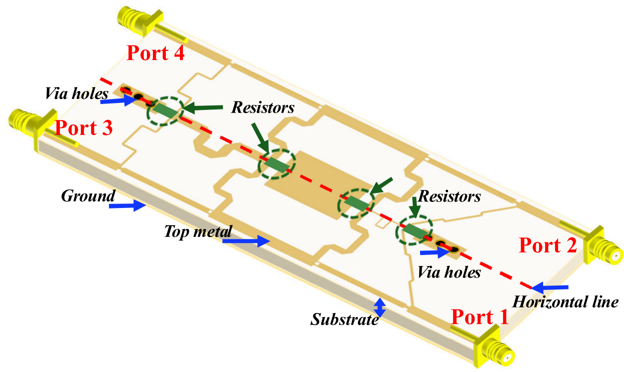


**FIGURE 2.** The 3D structure of the proposed A-CMF on the substrate of RO4350B.

In this paper, a bidirectional A-CMF is proposed and fabricated in a two-layer PCB using three-stage microstrip lines and four resistors. By adopting interdigitated coupled lines to replace the normal double parallel-coupled lines, the A-CMF can be easily manufactured. The introduced resistors in the symmetrical horizontal line dissipate CM noises into heat without affecting DM filtering performance. Using the even- and odd-mode design approach, the equivalent even- and odd-mode bisections and the constraint rules are obtained, while the effect of the main circuit parameters is thoroughly analyzed. Finally, the circuit prototype is simulated, fabricated, and the measured results agree well with the full wave EM simulation results. It is worth mentioning that this A-CMF realizes a wide absorption band with 90% absorption efficiency of CM noises from 2.18 GHz to 4.97 GHz.

## II. PROPOSED STRUCTURE AND ANALYSIS

The 3D structure of the proposed A-CMF is exhibited in Fig. 2. It's a four-port balanced-to-balanced differential structure, where the signals flow into the right differential input ports and flow out of the left differential output ports. The differential signals flowing into the structure is filtered but the CM noises flowing into the model is absorbed by the resistors.

### A. CONCEPT OF A-CMF

For a unidirectional A-CMF, the CM scattering parameters (S-parameters) $|S_{CC11}|$ and $|S_{CC21}|$ at the operating frequency need to be zero. $|S_{CC11}|$ being zero means that the CM noises are dissipated inner the structure instead of being reflected at the input ports. $|S_{CC21}|$ being zero promises the CM noises are attenuated and failed to be transmitted. Under these requirements, resistors are necessary in the CM equivalent circuit. For a bidirectional A-CMF, an extra CM S-parameter $|S_{CC22}|$ at the operating frequency is demanded to be zero. $|S_{CC22}|$ being zero means that the CM noises are dissipated inner the structure instead of being reflected at the output ports.

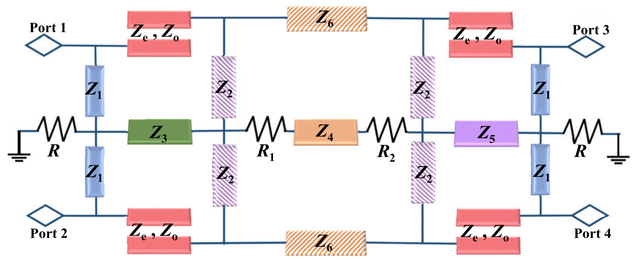


**FIGURE 3.** The circuit structure of the proposed A-CMF.

In addition, the DM S-parameter $|S_{DD11}|$ need to be zero and $|S_{DD21}|$ to be 1 to protect the integrity of the DM signals from attenuation. Moreover, the CM noise absorption efficiency is defined by 1-$|S_{CC11}|^2$-$|S_{CC21}|^2$, which can represent the absorption ability of the A-CMF.

### B. PROPOSED STRUCTURE

The circuit structure of the novel A-CMF is indicated in Fig. 3. It is a three-stage architecture symmetric with respect to the horizontal line. The differential input ports are defined by ports 1 and 2 and the differential output ports are defined by ports 3 and 4. The first- and third-stage are comprised of coupled lines with the even- and odd-mode characteristic impedances of $Z_e$ and $Z_o$ and branch lines with the characteristic impedances of $Z_1$, $Z_2$, $Z_3$, and $Z_5$, respectively. The second middle stage is consisted of branch lines with the characteristic impedances of $Z_4$ and $Z_6$ cascaded with two resistors $R_1$ and $R_2$. Extra two grounded resistors $R$ are located at the first- and third-stage for CM noise absorption. All the electrical lengths of the microstrip lines are selected as $\theta$ (=90°) at the operating frequency.

As the proposed circuit structure is a reciprocal four-port network, the mixed S-parameters matrix ($S^m$) can be represented by the single-ended S-parameters matrix ($S^{std}$) [22].

$$S^m = AS^{std}A^{-1} \tag{1-a}$$

$$S^m = \begin{bmatrix} S_{DD11} & S_{DD12} & S_{DC11} & S_{DC12} \\ S_{DD21} & S_{DD22} & S_{DC21} & S_{DC22} \\ S_{CD11} & S_{CD12} & S_{CC11} & S_{CC12} \\ S_{CD21} & S_{CD22} & S_{CC21} & S_{CC22} \end{bmatrix} \tag{1-b}$$

$$A = \frac{1}{\sqrt{2}} \begin{bmatrix} 1 & -1 & 0 & 0 \\ 0 & 0 & 1 & -1 \\ 1 & 1 & 0 & 0 \\ 0 & 0 & 1 & 1 \end{bmatrix} \tag{1-c}$$

$$S^{std} = \begin{bmatrix} S_{11} & S_{12} & S_{13} & S_{14} \\ S_{21} & S_{22} & S_{23} & S_{24} \\ S_{31} & S_{32} & S_{33} & S_{34} \\ S_{41} & S_{42} & S_{43} & S_{44} \end{bmatrix} \tag{1-d}$$

For an A-CMF, the CM conditions should be satisfied by the following (2). Noting that (2-a) is for bidirectional A-CMF and (2-b) is for unidirectional A-CMF. Additionally, the DM conditions are restricted by (3).

$$|S_{CC11}| = |S_{CC22}| = |S_{CC21}| = |S_{CC12}| = 0 \tag{2-a}$$

$$|S_{CC11}| = |S_{CC21}| = |S_{CC12}| = 0 \tag{2-b}$$
$$|S_{DD11}| = |S_{DD22}| = 0 \tag{3-a}$$
$$|S_{DD21}| = |S_{DD12}| = 1 \tag{3-b}$$

The following derivations take the bidirectional A-CMF for example. Supposed that DM signals (CM noises) will not convert into CM noises (DM signals). That is,

$$|S_{CD11}| = |S_{CD22}| = |S_{CD21}| = |S_{CD12}| = 0 \tag{4-a}$$
$$|S_{DC11}| = |S_{DC22}| = |S_{DC21}| = |S_{DC12}| = 0 \tag{4-b}$$

Based on (2-a), (3), and (4), the S-parameters matrix of the four-port network can be simplified.

$$S^{std} = \begin{bmatrix} 0 & 0 & -S_{41} & S_{41} \\ 0 & 0 & S_{41} & -S_{41} \\ -S_{41} & S_{41} & 0 & 0 \\ S_{41} & -S_{41} & 0 & 0 \end{bmatrix} \tag{5}$$

Finally, the S-parameters matrix of the even- and odd-mode equivalent circuit are acquired.

$$S_{even} = \begin{bmatrix} S_{CC11} & S_{CC12} \\ S_{CC21} & S_{CC22} \end{bmatrix} = \begin{bmatrix} 0 & 0 \\ 0 & 0 \end{bmatrix} \tag{6-a}$$
$$S_{odd} = \begin{bmatrix} S_{DD11} & S_{DD12} \\ S_{DD21} & S_{DD22} \end{bmatrix} = -2S_{41}\begin{bmatrix} 0 & 1 \\ 1 & 0 \end{bmatrix} \tag{6-b}$$

### C. DIFFERENTIAL-MODE ANALYSIS

Under the DM signals excitation, the symmetrical horizontal line is a perfect electrical wall and the corresponding odd-mode equivalent circuit is depicted in Fig. 4(a). There is no current flowing into the resistors. The electrical lengths of all the microstrip lines are quarter of wavelength at the operating frequency.

The equivalent DM basic circuit as an inset in Fig. 4(b) consists of a branch line with the characteristic impedance of $Z_6$ and two cascaded double parallel-coupled lines with the even- and odd-mode characteristic impedances of $Z_e$ and $Z_o$. This equivalent basic circuit is similar with the SIR introducing three transmission poles in the passband [27]. The simulated results of the basic circuit at 3.5 GHz are provided in Fig. 4(b). The four resonant frequencies with the $|S_{DD11}|$ valleys are observed at 2.3 GHz ($f_{TZ3}$), 3.1 GHz ($f_{TZ1}$), 3.9 GHz ($f_{TZ2}$), and 4.7 GHz ($f_{TZ4}$), respectively.

Compared with the basic circuit, a pair of short-ended stubs with the characteristic impedance of $Z_2$ are paralleled at the two sides of the middle line constructing a pair of extra transmission zeros (TZs). By introducing a pair of short-ended stubs with the characteristic impedance of $Z_1$ shunted in the input and output ports, two additional TZs are achieved. The odd-mode equivalent circuit can be categorized as a stub-loaded multiple-mode resonator. Therefore, the circuit simulations of the multiple-mode resonance behaviors are shown in Fig. 5 and the corresponding circuit parameters are listed in Table 1.

In Fig. 5, seven resonant frequencies with the valleys of $|S_{DD11}|$ are observed at 1.1 GHz ($f_{TZ6}$), 1.4 GHz ($f_{TZ4}$), 2.2 GHz ($f_{TZ2}$), 3.5 GHz ($f_{TZ1}$), 4.8 GHz ($f_{TZ3}$), 5.6 GHz ($f_{TZ5}$),

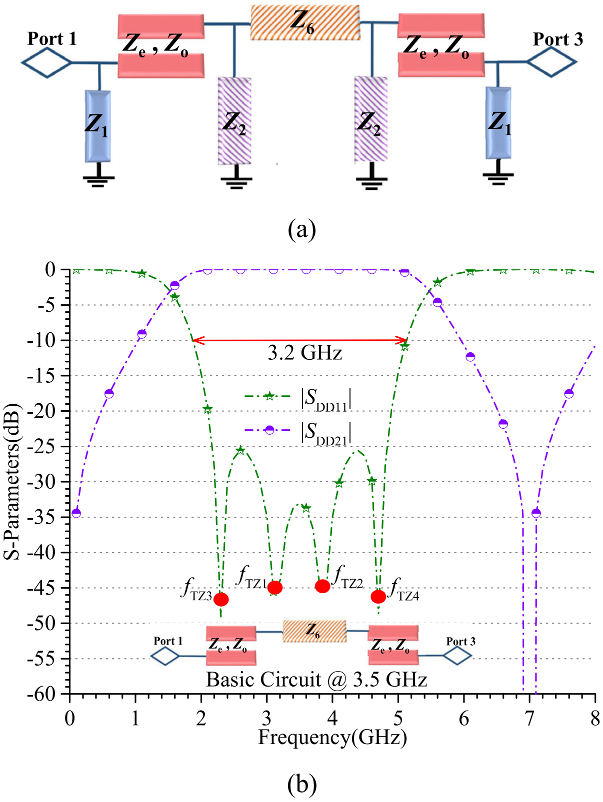


**FIGURE 4.** (a) Equivalent circuit of the proposed A-CMF under the DM signals excitation and (b) the circuit simulations of the DM basic circuit.

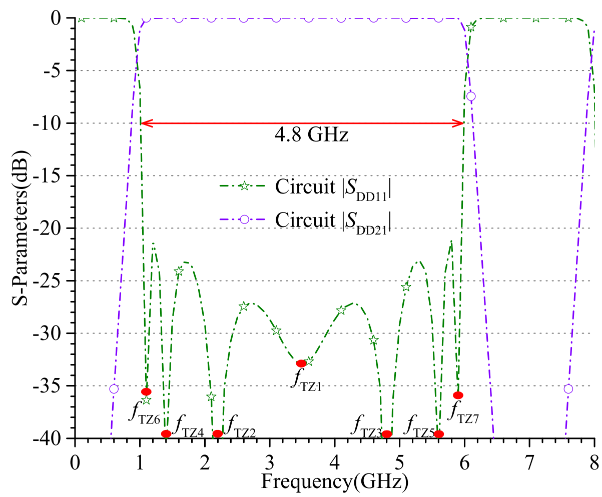


**FIGURE 5.** The ideal circuit simulations of the A-CMF with the DM responses $|S_{DD11}|$ and $|S_{DD21}|$.

and 5.9 GHz ($f_{TZ7}$), respectively. The three TZs of $f_{TZ2}$, $f_{TZ1}$, and $f_{TZ3}$ are brought out by the basic circuit, $f_{TZ6}$ and $f_{TZ7}$ are introduced by the shorted stubs with the impedance of $Z_2$, $f_{TZ4}$ and $f_{TZ5}$ are contributed by the shorted stubs with the impedance of $Z_1$. Observed from the equation (6-b) and the simulations, the odd-mode equivalent half-circuit is a bandpass filter.

To investigate the frequency responses of the odd-mode half-circuit, the circuit parameters of $Z_e$, $Z_o$, and $Z_6$ are

**TABLE 1. The circuit parameters of the A-CMF with double parallel-coupled lines.**

| A-CMF with Double Parallel-Coupled Lines | |
|---|---|
| $Z_1$, $Z_2$, $Z_3$, $Z_4$, $Z_5$, $Z_6$, $Z_e$, $Z_o$, $R_1$, $R_2$, $R$ | $\theta$ @ 3.5 GHz |
| 119 Ω, 86 Ω, 88 Ω, 21 Ω, 104 Ω, 46 Ω, 120 Ω, 23 Ω,29 Ω, 20 Ω, 150 Ω | 90° |

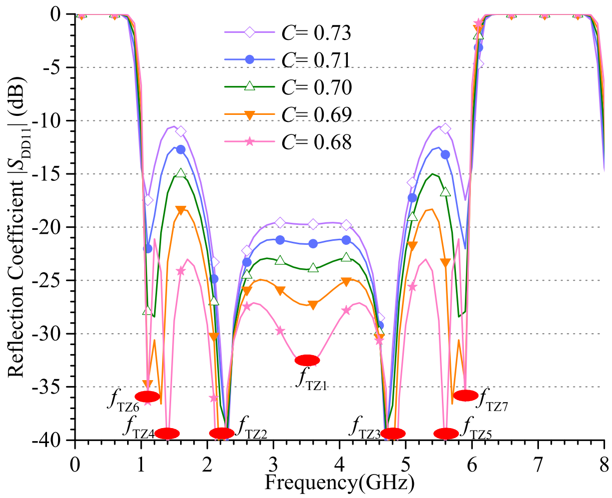


(a)

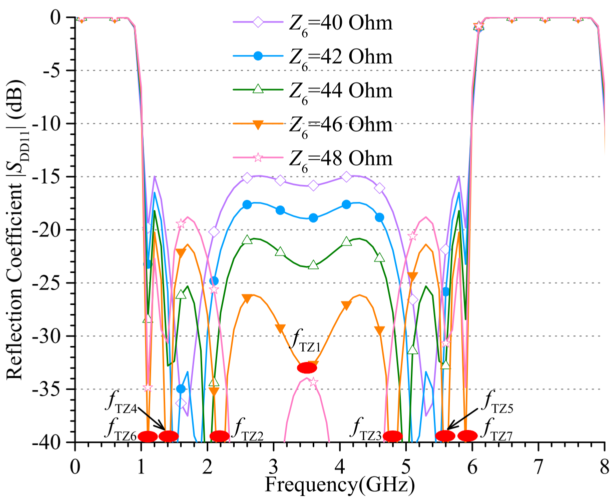


(b)

**FIGURE 6. The ideal simulated reflection coefficient $|S_{DD11}|$ of the A-CMF with different circuit parameters: (a) different coupling coefficient of $C$, (b) different characteristic impedance of $Z_6$.**

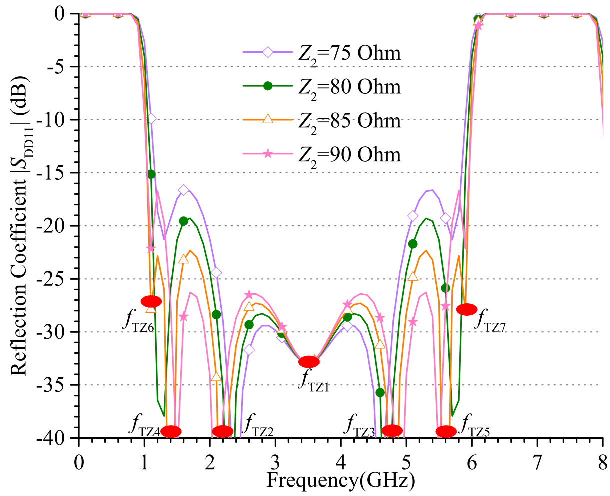


(a)

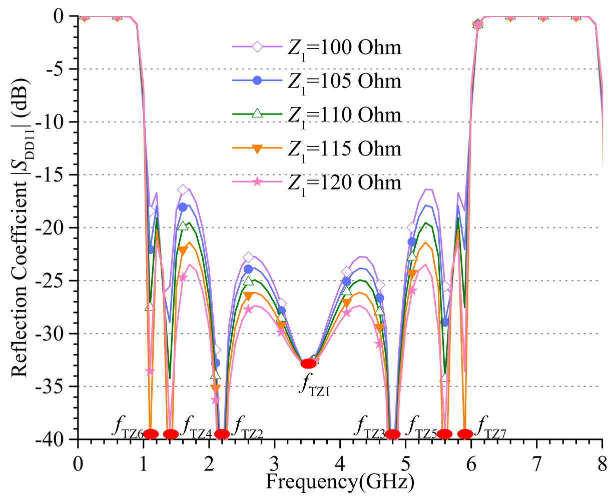


(b)

**FIGURE 7. The ideal simulated reflection coefficient $|S_{DD11}|$ of the A-CMF with different circuit parameters: (a) different characteristic impedance of $Z_2$, (b) different characteristic impedance of $Z_1$.**

selected with various values shown in Fig. 6. The coupling coefficient is defined by $C$, which equals to $(Z_e\text{-}Z_o)/(Z_e+Z_o)$. As $C$ decreases, the reflection coefficient $|S_{DD11}|$ is lower. The two adjacent TZs of $f_{TZ4}$ and $f_{TZ6}$ merge into a TZ located in the left as the similar with the two adjacent TZs of $f_{TZ5}$ and $f_{TZ7}$ merge into a TZ located in the right. The middle $f_{TZ1}$ disappears as $C$ increases. In Fig. 6(b), the simulated $|S_{DD11}|$ decreases among $f_{TZ2}$ and $f_{TZ3}$, $f_{TZ6}$ and $f_{TZ4}$, $f_{TZ5}$ and $f_{TZ7}$ but increases separately among $f_{TZ4}$ and $f_{TZ2}$, $f_{TZ3}$ and $f_{TZ5}$ while the impedance $Z_6$ increases.

To provide a quantitative view on the effect of the two pairs of the shunted stubs, the frequency responses with different characteristic impedances of the stubs can be observed from Fig. 7. The locations of the resonant frequency points are constant so long as the electrical lengths are 90° without change. In Fig. 7(a), the DM reflection coefficient $|S_{DD11}|$ increases between $f_{TZ2}$ and $f_{TZ3}$ but decreases between $f_{TZ4}$ and $f_{TZ2}$, $f_{TZ3}$ and $f_{TZ5}$ while the characteristic impedance of $Z_2$ increases. Fig. 7(b) illustrates the DM reflection coefficient $|S_{DD11}|$ decreases with the characteristic impedance of $Z_1$ increases.

### D. COMMON-MODE ANALYSIS

Under the CM signals excitation, the symmetrical horizontal line is a perfect magnetic wall and the corresponding

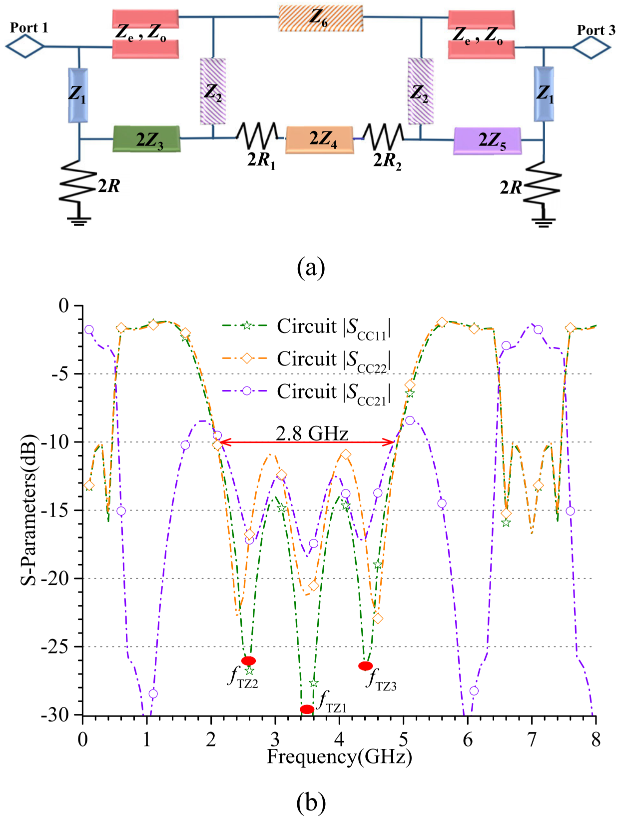


**FIGURE 8.** **(a) Equivalent circuit of the proposed A-CMF under the CM signals excitation and (b) the CM responses $|S_{CC11}|$, $|S_{CC21}|$, and $|S_{CC22}|$.**

even-mode equivalent circuit is shown in Fig. 8(a). The resistances and the characteristic impedances of the microstrip lines in the symmetrical line are twice of the original values. Besides, the electrical lengths of all the microstrip lines are selected as 90° at the operating frequency. Furthermore, based on the corresponding circuit parameters listed in Table 1, the CM responses at 3.5 GHz with bidirectional absorption are plotted in Fig. 8(b). There are three TZs at 2.6 GHz ($f_{TZ2}$), 3.5 GHz ($f_{TZ1}$), and 4.4 GHz ($f_{TZ3}$), respectively.

Observed from Fig. 9, the characteristic impedance of $Z_4$ is a main variable affecting the CM absorption responses. Moreover, the resistors $R_1$ and $R_2$ independently influence the input CM absorption and the output CM absorption. The resistors $R$ effect both input and output CM responses. All these variables only influence the CM responses without any effect on the DM filtering responses. Fig. 9 illustrates that the insertion loss $|S_{CC21}|$ and the input and output reflection coefficient $|S_{CC11}|$ and $|S_{CC22}|$ all decrease with $Z_4$ increases. In addition, the TZs $f_{TZ2}$ and $f_{TZ3}$ gather to the middle $f_{TZ1}$ with $Z_4$ increases.

In Fig. 10(a), the CM input reflection coefficient $|S_{CC11}|$ decreases while the resistance $R_1$ decreases and the CM output reflection coefficient $|S_{CC22}|$ decreases while the resistance $R_2$ decreases given in Fig. 10(b). The TZs $f_{TZ2}$ and

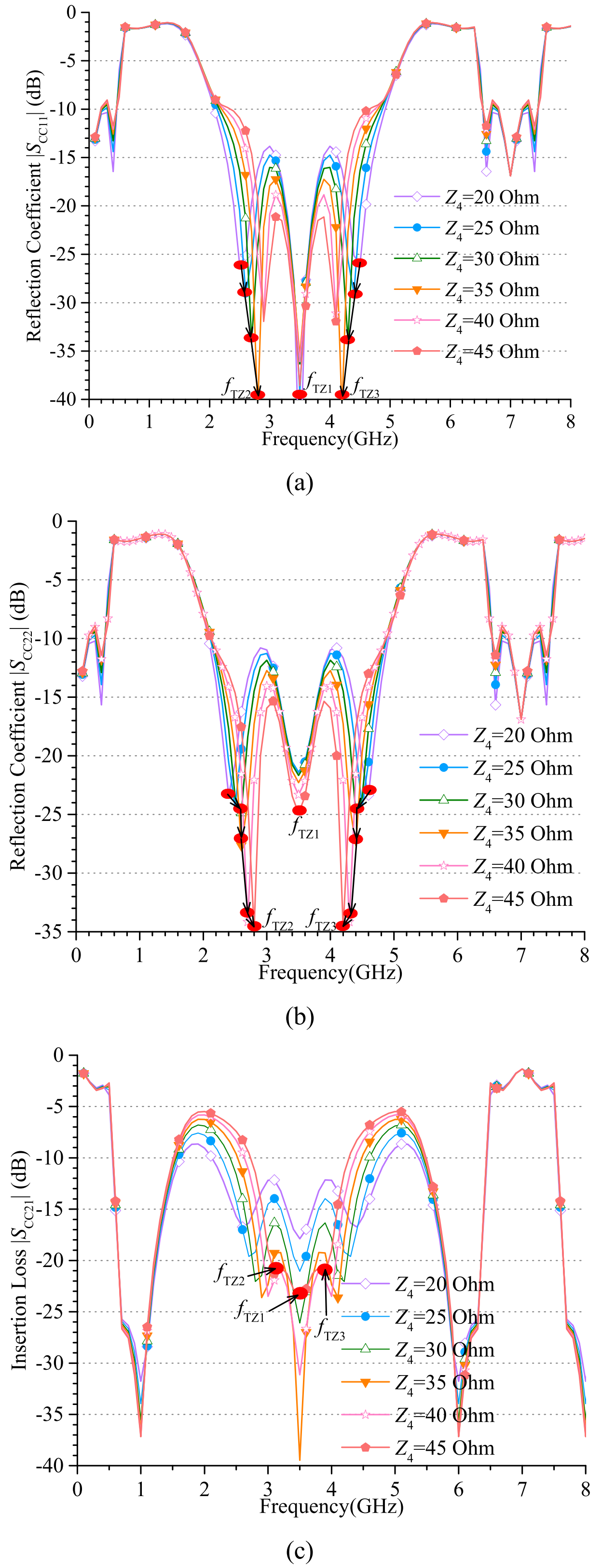


**FIGURE 9.** **The ideal simulated CM responses of the A-CMF with different characteristic impedance of $Z_4$: (a) the input reflection coefficient $|S_{CC11}|$, (b) the output reflection coefficient $|S_{CC22}|$, (c) the insertion loss $|S_{CC21}|$.**

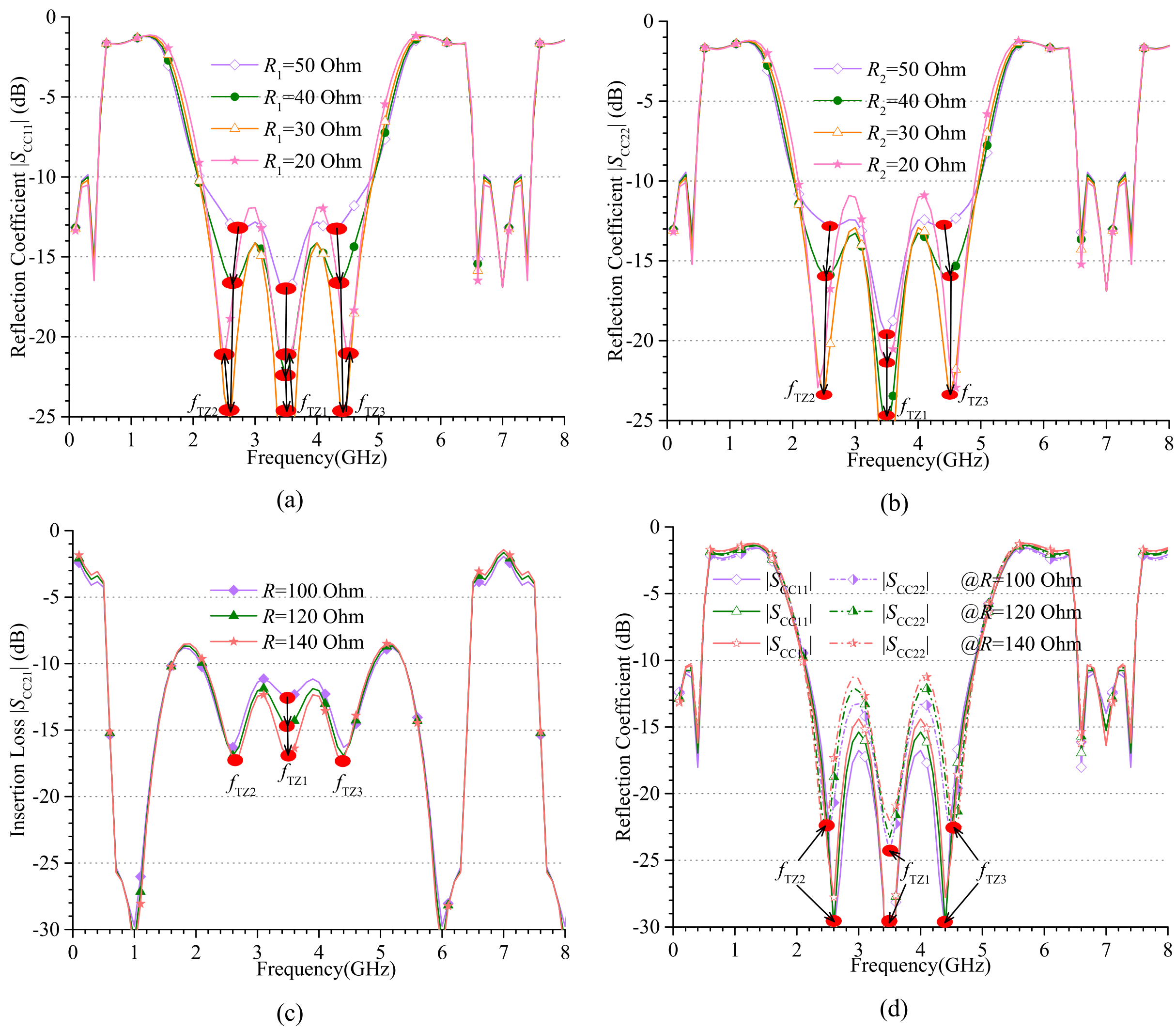


**FIGURE 10.** **The ideal simulated CM responses of the A-CMF with different resistors of $R_1$, $R_2$, $R$: (a) the input reflection coefficient $|S_{CC11}|$ with different $R_1$, (b) the output reflection coefficient $|S_{CC22}|$ with different $R_2$, (c) the insertion loss $|S_{CC21}|$ with different $R$, (d) the input and output reflection coefficient $|S_{CC11}|$ and $|S_{CC22}|$ with different $R$.**

**TABLE 2.** **Performance comparison of the A-CMF.**

| Refs. | Fabrication | CM-Stopband (GHz) | CM-ABW (GHz) | DM-BW (GHz) | Absorption | Years |
|---|---|---|---|---|---|---|
| [22] | PCB (2-layer) | 1.51-2.62 | 80% (1.51-2.62) | 1.51-2.62 | Resistor (N/A) | 2017 |
| [23] | PCB (4-layer) | 2.0-2.3 | 95% (2.1-2.2) | 0->5 | Resistor (U) | 2017 |
| [24] | PCB (4-layer) | 2.4-2.7* | 90% (2.4-2.5) | 0-7 | Substrate (N/A) | 2018 |
| [25] | PCB (4-layer) | 1.7-7.0* | 95% (1.9-4.1) | 0-6.4 | Resistor (N/A) | 2019 |
| [26] | PCB (2-layer)<br>PCB (2-layer) | 1.7->7.5<br>1.7-4.2 | 80% (1.8-3.0)<br>80% (1.8-3.0) | 0-7.4<br>0-7.4 | Resistor (B)<br>Resistor (U) | 2019 |
| This work | PCB (2-layer) | 0.72->8 | 90% (2.18-4.97) | 1.38-5.19 | Resistor (B) | 2019 |

CM-Stopband: defined by $|S_{CC21}| < -10$ dB. CM-ABW: defined by the corresponding absorption efficiency $1-|S_{CC11}|^2-|S_{CC21}|^2$. DM-BW: defined by $0>|S_{DD21}|> -3$ dB. U: Unidirectional. B: Bidirectional. *: Estimated value.

$f_{TZ3}$ keep away from the middle $f_{TZ1}$ with $R_1$ and $R_2$ decrease. Demonstrated in Fig. 10(c) and Fig. 10(d), $|S_{CC21}|$ slightly decreases but $|S_{CC11}|$ and $|S_{CC22}|$ increase with the resistor $R$ increases.

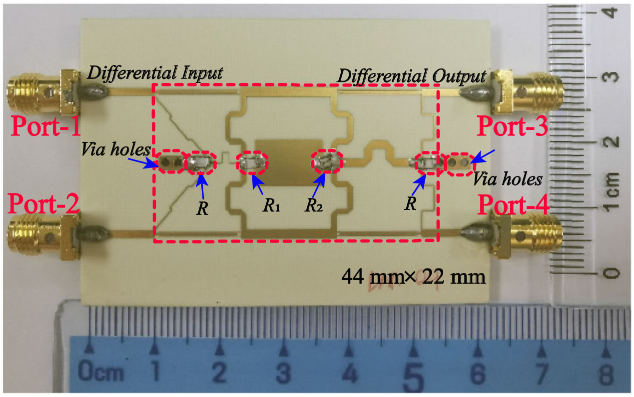


**FIGURE 11.** The photograph of the fabricated A-CMF. The differential input and differential output ports are terminated with 50-Ω SMA connectors and the via holes are used for the ground connection. The resistors $R_1$, $R_2$, and $R$ are selected as 20 Ω, 22 Ω, and 100 Ω.

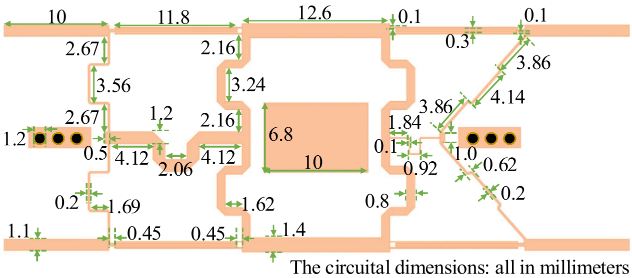


**FIGURE 12.** The circuit dimensions of the proposed A-CMF.

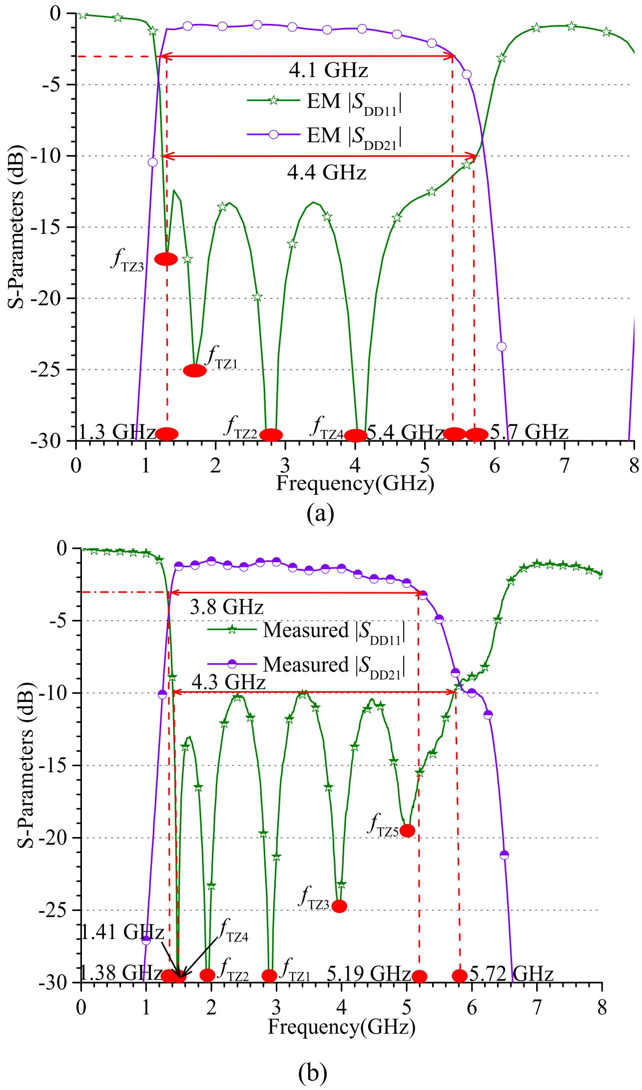


**FIGURE 13.** The EM simulated and measured results of the proposed A-CMF: (a) the EM simulated DM responses $|S_{DD11}|$ and $|S_{DD21}|$, (b) the measured DM responses $|S_{DD11}|$ and $|S_{DD21}|$.

## III. IMPLEMENTATION AND EXPERIMENTAL RESULTS

In this paper, a bidirectional A-CMF operating at 3.5 GHz for 5G "green" communications is implemented. The design steps are summarized as follows:

1. Determine the operating frequency point $f_0$ as 3.5 GHz.
2. Determine the impedance parameters of $Z_e$, $Z_o$, $Z_1$, $Z_2$, and $Z_6$ according to the expected DM filtering responses.
3. Determine the impedance and resistance parameters of $Z_3$, $Z_4$, $Z_5$, $R$, $R_1$, and $R_2$ to acquire expected CM absorption responses.

Following the above steps, the ideal electrical parameters of the proposed A-CMF are listed in Table 1. Since the interdigitated coupled lines with enhanced degree of coupling are used to make up the filter with better return loss in the wide passband [28]. Thus, for easy manufacturing and enhanced coupling, interdigitated coupled lines are adopted to replace the normal double parallel-coupled lines.

### A. IMPLEMENTATION

To prove the above theory, the proposed A-CMF is simulated and fabricated on the substrate of Rogers 4350B with the relative dielectric constant of 3.66, the loss tangent of 0.0037, and the thickness of 0.508 mm. By properly designing, the structure parameters and the size of the proposed filter are optimized using Advanced Design System (ADS). The photograph of the fabricated A-CMF is given in Fig. 11. The corresponding circuit dimensions are displayed in Fig. 12. Additionally, the via holes are used as grounded holes. The whole dimension of this manufactured A-CMF is approximately 44 mm × 22 mm. Then, the circuit prototype is measured using a four-port ZVA8 vector network analyzer.

### B. DIFFERENTIAL-MODE FILTERING RESPONSE

The EM simulated results of the DM responses are shown in Fig. 13(a). The 3-dB bandwidth of $|S_{DD21}|$ is from 1.3 GHz to 5.4 GHz realizing good selectivity of this filter. The EM simulated return loss $|S_{DD11}|$ is better than 10 dB from 1.3 GHz to 5.7 GHz. In Fig. 13(b), the measured results show that the DM signals can pass through this A-CMF almost without being attenuated from 1.38 GHz to 5.19 GHz. The bandwidth of $|S_{DD11}|$ lower than −10 dB is from 1.41 GHz to 5.72 GHz.

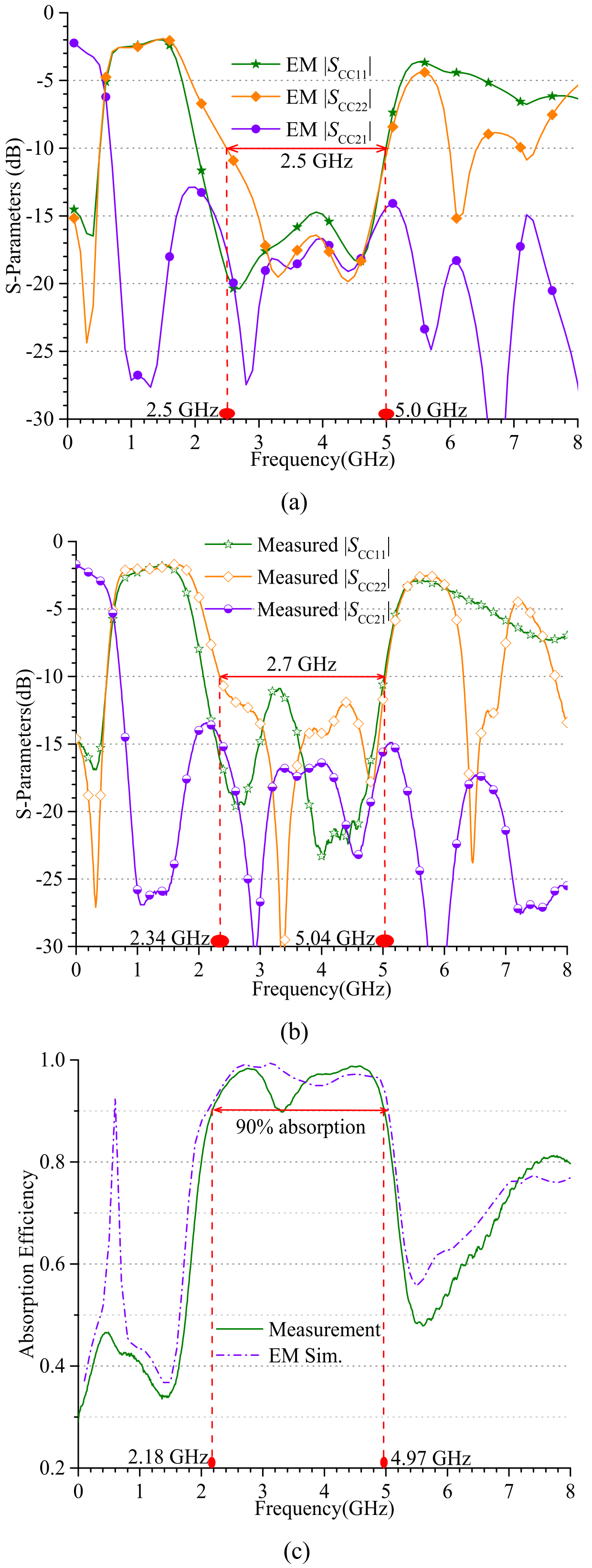


**FIGURE 14.** **The EM simulated and measured results of the proposed A-CMF: (a) the EM simulated CM responses $|S_{CC11}|$, $|S_{CC21}|$, and $|S_{CC22}|$, (b) the measured CM responses $|S_{CC11}|$, $|S_{CC21}|$, and $|S_{CC22}|$, (c) the absorption efficiency 1-$|S_{CC11}|^2$-$|S_{CC21}|^2$.**

### C. COMMON-MODE NOISE SUPPRESSION AND ABSORPTION

The EM simulated and measured results of the CM responses are shown in Fig. 14. The EM simulated CM absorption bandwidth is from 2.5 GHz to 5.0 GHz under the conditions that the $|S_{CC11}|$, $|S_{CC22}|$, and $|S_{CC21}|$ are all lower than $-10$ dB. In Fig. 14(b), the measured $|S_{CC21}|$ is below $-10$ dB from 0.72 GHz to 8 GHz, which means the CM noises are suppressed through a broad band. The measured CM return loss $|S_{CC11}|$ at the input port is below $-10$ dB from 2.08 GHz to 5.02 GHz, which means the noises are absorbed by the resistors instead of being reflected to the previous block. The measured CM return loss $|S_{CC22}|$ at the output port is below $-10$ dB from 2.34 GHz to 5.04 GHz. It is worth noting that this A-CMF realizes a wide absorption band with 90% absorption efficiency of CM noises from 2.18 GHz to 4.97 GHz plotted in Fig. 14(c).

### D. PERFORMANCE COMPARISON WITH STATES-OF-THE-ART A-CMFS

Finally, the performances of the proposed bidirectional A-CMF are compared with the related previous A-CMFs, as summarized in Table 2. It is seen that the proposed circuit is fabricated in a simple two-layer PCB with bidirectional absorption, good DM transmission, wideband CM suppression, and high CM absorption efficiency through a broad bandwidth. Among all the listed A-CMFs, the adopted fabrication process of a two-layer PCB is simple and cost-efficient in [22], [26]. But the operating bandwidth and the absorption efficiency both have great space to improve. Latest, two circuits are presented with bidirectional absorption and unidirectional absorption, respectively. The DM bandwidth is quite broad but the CM absorption efficiency is only 80 % from 1.8 GHz to 3.0 GHz [26]. These A-CMFs achieve a high absorption efficiency for unidirectional CM noise absorption but are fabricated in a complex four-layer PCB [23]–[25].

## IV. CONCLUSION

A novel bidirectional A-CMF in a two-layer PCB is proposed with wide CM stopband, high CM absorption efficiency, wide CM absorption bandwidth, and good DM transmission responses. The interdigitated coupled lines are introduced to replace the normal double parallel-coupled lines for enhanced coupling and easy manufacture. The function of absorbing the CM noises from both directions within a broad band can be widely used for 5G "green" communications and several differential communication systems with high demand of electromagnetic compatibility.

## REFERENCES

[1] L. Liu and W. Yu, "Massive connectivity with massive MIMO—Part I: Device activity detection and channel estimation," *IEEE Trans. Signal Process.*, vol. 66, no. 11, pp. 2933–2946, Jun. 2018.

[2] T.-H. Lin, J. Bito, J. G. D. Hester, J. Kimionis, R. A. Bahr, and M. M. Tentzeris, "On-body long-range wireless backscattering sensing system using inkjet-/3-D-printed flexible ambient RF energy harvesters capable of simultaneous DC and harmonics generation," *IEEE Trans. Microw. Theory Techn.*, vol. 65, no. 12, pp. 5389–5400, Dec. 2017.

[3] J. Bito, J. G. Hester, and M. M. Tentzeris, "Ambient RF energy harvesting from a two-way talk radio for flexible wearable wireless sensor devices utilizing inkjet printing technologies," *IEEE Trans. Microw. Theory Techn.*, vol. 63, no. 12, pp. 4533–4543, Dec. 2015.

[4] M. Arrawatia, M. Baghini, and G. Kumar, "Broadband bent triangular omnidirectional antenna for RF energy harvesting," *IEEE Antennas Wireless Propag. Lett.*, vol. 15, pp. 36–39, 2015.

[5] Y. Guan, Y. Wu, M. Li, W. Wang, and Y. Liu, "Generalised MIT in a tri-band LNA," *IET Microw., Antennas Propag.*, vol. 11, no. 2, pp. 294–302, Jan. 2017.

[6] S. Kim and K. Kwon, "A 50-MHz–1-GHz 2.3-dB NF noise-cancelling balun-LNA employing a modified current-bleeding technique and balanced loads," *IEEE Trans. Circuits Syst. I*, vol. 66, no. 2, pp. 546–554, Feb. 2019.

[7] F. Declercq and H. Rogier, "Active integrated wearable textile antenna with optimized noise characteristics," *IEEE Trans. Antennas Propag.*, vol. 58, no. 9, pp. 3050–3054, Sep. 2010.

[8] F. Bilotti, L. Di Palma, D. Ramaccia, and A. Toscano, "Self-filtering low-noise horn antenna for satellite applications," *IEEE Antennas Wireless Propag. Lett.*, vol. 11, pp. 354–357, 2012.

[9] J. Shi and Q. Xue, "Dual-band and wide-stopband single-band balanced bandpass filters with high selectivity and common-mode suppression," *IEEE Trans. Microw. Theory Techn.*, vol. 58, no. 8, pp. 2204–2212, Aug. 2010.

[10] Y. C. Li and Q. Xue, "Tunable balanced bandpass filter with constant bandwidth and high common-mode suppression," *IEEE Trans. Microw. Theory Techn.*, vol. 59, no. 10, pp. 2452–2460, Oct. 2011.

[11] X.-H. Wu and Q.-X. Chu, "Compact differential ultra-wideband bandpass filter with common-mode suppression," *IEEE Microw. Wireless Compon. Lett.*, vol. 22, no. 9, pp. 456–458, Sep. 2012.

[12] W. Feng, W. Che, and Q. Xue, "Balanced filters with wideband common mode suppression using dual-mode ring resonators," *IEEE Trans. Circuits Syst. I, Reg. Papers*, vol. 62, no. 6, pp. 1499–1507, Jun. 2015.

[13] L.-H. Zhou, Y.-L. Ma, J. Shi, J.-X. Chen, and W. Che, "Differential dual-band bandpass filter with tunable lower band using embedded DGS unit for common-mode suppression," *IEEE Trans. Microw. Theory Techn.*, vol. 64, no. 12, pp. 4183–4191, Dec. 2016.

[14] Y. Song, H. W. Liu, W. Zhao, P. Wen, and Z. Wang, "Compact balanced dual-band bandpass filter with high common-mode suppression using planar via-free CRLH resonator," *IEEE Microw. Wireless Compon. Lett.*, vol. 28, no. 11, pp. 996–998, Nov. 2018.

[15] W. Zhang, Y. Liu, Y. Wu, A. Hasan, F. M. Ghannouchi, Y. Zhao, X. Du, and W. Chen, "Novel planar compact coupled-line single-ended-to-balanced power divider," *IEEE Trans. Microw. Theory Techn.*, vol. 65, no. 8, pp. 2953–2963, Aug. 2017.

[16] W. Feng, Y. Zhao, W. Che, R. Gomez-Garcia, and Q. Xue, "Single-ended-to-balanced filtering power dividers with wideband common-mode suppression," *IEEE Trans. Microw. Theory Techn.*, vol. 66, no. 12, pp. 5531–5542, Dec. 2018.

[17] F. Huang, J. Wang, J. Hong, and W. Wu, "A new balanced-to-unbalanced filtering power divider with dual controllable passbands and enhanced in-band common-mode suppression," *IEEE Trans. Microw. Theory Techn.*, vol. 67, no. 2, pp. 695–703, Feb. 2019.

[18] C.-Y. Hsiao, C.-H. Cheng, and T.-L. Wu, "A new broadband common-mode noise absorption circuit for high-speed differential digital systems," *IEEE Trans. Microw. Theory Techn.*, vol. 63, no. 6, pp. 1894–1901, Jun. 2015.

[19] S. Chen, W.-C. Lee, and T.-L. Wu, "A balanced-to-balanced power divider with common-mode noise absorption," in *IEEE MTT-S Int. Microw. Symp. Dig.*, San Francisco, CA, USA, May 2016, pp. 1–4.

[20] B. Xia, L.-S. Wu, and J.-F. Mao, "An Absorptive balanced-to-balanced power divider," *IEEE Access*, vol. 6, pp. 14613–14619, 2018.

[21] S. Chen, W.-C. Lee, and T.-L. Wu, "Balanced-to-balanced and balanced-to-unbalanced power dividers with ultra-wideband common-mode rejection and absorption based on mode-conversion approach," *IEEE Trans. Compon., Packag. Manufact. Technol.*, vol. 9, no. 2, pp. 306–316, Feb. 2019.

[22] W. Zhang, Y. Wu, Y. Liu, C. Yu, A. Hasan, and F. M. Ghannouchi, "Planar wideband differential-mode bandpass filter with common-mode noise absorption," *IEEE Microw. Wireless Compon. Lett.*, vol. 27, no. 5, pp. 458–460, May 2017.

[23] P.-J. Li, Y.-C. Tseng, C.-H. Cheng, and T.-L. Wu, "A novel absorptive common-mode filter for cable radiation reduction," *IEEE Trans. Compon., Packag. Manufact. Technol.*, vol. 7, no. 4, pp. 511–518, Apr. 2017.

[24] P.-J. Li, C.-H. Cheng, and T.-L. Wu, "A resistor-free absorptive common-mode filter using gap-coupled resonator," *IEEE Microw. Wireless Compon. Lett.*, vol. 28, no. 10, pp. 885–887, Oct. 2018.

[25] P.-J. Li and T.-L. Wu, "Synthesized method of dual-band common-mode noise absorption circuits," *IEEE Trans. Microw. Theory Techn.*, vol. 67, no. 4, pp. 1392–1401, Apr. 2019.

[26] C.-H. Cheng and T.-L. Wu, "Analysis and design method of a novel absorptive common-mode filter," *IEEE Trans. Microw. Theory Techn.*, vol. 67, no. 5, pp. 1826–1835, May 2019.

[27] L. Zhu, S. Sun, and W. Menzel, "Ultra-wideband (UWB) bandpass filters using multiple-mode resonator," *IEEE Microw. Wireless Compon. Lett.*, vol. 15, no. 11, pp. 796–798, Nov. 2005.

[28] S. Sun and L. Zhu, "Capacitive-ended interdigital coupled lines for UWB bandpass filters with improved out-of-band performances," *IEEE Microw. Wireless Compon. Lett.*, vol. 16, no. 8, pp. 440–442, Aug. 2006.

**YANGYANG GUAN** received the B.Eng. degree in electronic engineering from the Chongqing University of Posts and Telecommunications (CQUPT), Chongqing, China, in 2014. She is currently pursuing the Ph.D. degree in electronic engineering with the Beijing University of Posts and Telecommunications (BUPT), Beijing, China.

From February, 2018 to February, 2019, she was a Joint Ph.D. Student with the Georgia Institute of Technology, Atlanta, USA. Her research interests include microwave low noise amplifiers, power dividers, antennas, and filters design.

**YONGLE WU** (Senior Member, IEEE) received the B.Eng. degree in communication engineering and the Ph.D. degree in electronic engineering from the Beijing University of Posts and Telecommunications (BUPT), Beijing, China, in 2006 and 2011, respectively.

From April to October in 2010, he was a Research Assistant with the City University of Hong Kong (CityU), Hong Kong. In 2011, he joined the BUPT, where he is currently a Full Professor with the School of Electronic Engineering. His research interests include microwave components, circuits, antennas, and wireless systems design.

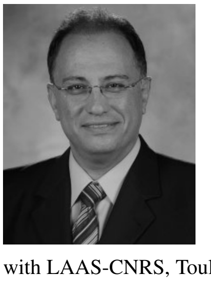

**MANOS M. TENTZERIS** (Fellow, IEEE) received the Diploma degree *(magna cum laude)* in electrical and computer engineering from the National Technical University of Athens, Athens, Greece, and the M.S. and Ph.D. degrees in electrical engineering and computer science from the University of Michigan, Ann Arbor, MI, USA.

He was a Visiting Professor with the Technical University of Munich, Munich, Germany, in 2002, with GTRI-Ireland, Athlone, Ireland, in 2009, and with LAAS-CNRS, Toulouse, France, in 2010. He is currently a Ken Byers Professor in flexible electronics with the School of Electrical and Computer Engineering, Georgia Institute of Technology, Atlanta, GA, USA, where he heads the ATHENA Research Group (20 researchers). He has served as the Head of the GTECE Electromagnetics Technical Interest Group, as the Georgia Electronic Design Center Associate Director of RFID/Sensors research, as the Georgia Institute of Technology NSF-Packaging Research Center Associate Director of RF Research, and as the RF Alliance Leader.

He has helped develop academic programs in 3-D/inkjet-printed RF electronics and modules, flexible electronics, origami and morphing electromagnetics, highly integrated/multilayer packaging for RF and wireless applications using ceramic and organic flexible materials, paper-based RFID's and sensors, wireless sensors and biosensors, wearable electronics, "Green" electronics, energy harvesting and wireless power transfer, nanotechnology applications in RF, microwave MEMs, and SOP-integrated (UWB, multiband, mmW, and conformal) antennas. He has authored more than 650 articles in refereed journals and conference proceedings, five books, and 25 book chapters.

Dr. Tentzeris is a member of the URSI-Commission D and the MTT-15 Committee, an Associate Member of EuMA, a Fellow of the Electromagnetic Academy, and a member of the Technical Chamber of Greece. He served as one of the IEEE MTT-S Distinguished Microwave Lecturers from 2010 to 2012 and is one of the IEEE CRFID Distinguished Lecturers. He was a recipient/co-recipient of the 2019 Humboldt Research Award, the 2018 Intel IEEE ECTC 2018 Best Student Paper Award, the 2017 Georgia Institute of Technology Outstanding Achievement in Research Program Development Award, the 2016 Bell Labs Award Competition 3rd Prize, the 2015 IET Microwaves, Antennas, and Propagation Premium Award, the 2014 Georgia Institute of Technology ECE Distinguished Faculty Achievement Award, the 2014 IEEE RFID-TA Best Student Paper Award, the 2013 IET Microwaves, Antennas and Propagation Premium Award, the 2012 FiDiPro Award in Finland, the iCMG Architecture Award of Excellence, the 2010 IEEE Antennas and Propagation Society Piergiorgio L. E. Uslenghi Letters Prize Paper Award, the 2011 International Workshop on Structural Health Monitoring Best Student Paper Award, the 2010 Georgia Institute of Technology Senior Faculty Outstanding Undergraduate Research Mentor Award, the 2009 IEEE Transactions on Components and Packaging Technologies Best Paper Award, the 2009 E. T. S. Walton Award from the Irish Science Foundation, the 2007 IEEE AP-S Symposium Best Student Paper Award, the 2007 IEEE MTT-S IMS Third Best Student Paper Award, the 2007 ISAP 2007 Poster Presentation Award, the 2006 IEEE MTT-S Outstanding Young Engineer Award, the 2006 Asia-Pacific Microwave Conference Award, the 2004 IEEE Transactions on Advanced Packaging Commendable Paper Award, the 2003 NASA Godfrey "Art" Anzic Collaborative Distinguished Publication Award, the 2003 IBC International Educator of the Year Award, the 2003 IEEE CPMT Outstanding Young Engineer Award, the 2002 International Conference on Microwave and Millimeter-Wave Technology Best Paper Award, Beijing, China, the 2002 Georgia Institute of Technology-ECE Outstanding Junior Faculty Award, the 2001 ACES Conference Best Paper Award, the 2000 NSF CAREER Award, and the 1997 Best Paper Award of the International Hybrid Microelectronics and Packaging Society. He was the Co-Chair of the 2019 IEEE APS Conference, a TPC Chair of the IEEE MTT-S IMS 2008 Symposium, and the Chair of the 2005 IEEE CEM-TD Workshop. He is the Vice-Chair of the RF Technical Committee (TC16) of the IEEE CPMT Society. He is the Founder and the Chair of the RFID Technical Committee (TC24) of the IEEE MTT-S and the Secretary/Treasurer of the IEEE C-RFID. He is also an Associate Editor of the IEEE TRANSACTIONS ON MICROWAVE THEORY AND TECHNIQUES, the IEEE TRANSACTIONS ON ADVANCED PACKAGING, and the *International Journal on Antennas and Propagation*. He has given more than 100 invited talks to various universities and companies all over the world.